

Zinc Sorption to Three Gram-Negative Bacteria: Combined Titration, Modeling, and EXAFS Study

V. GUINÉ,[†] L. SPADINI,[‡] G. SARRET,[‡]
M. MURIS,[§] C. DELOLME,[§]
J.-P. GAUDET,[†] AND J. M. F. MARTINS*[†]

Laboratoire d'Etude des Transferts en Hydrologie et Environnement (LTHE-UMR 5564) BP 53, 38041 Grenoble Cedex 9, France, Environmental Geochemistry Group, LGIT, University J. Fourier and CNRS, BP 53, 38041 Grenoble Cedex 9, France, and Laboratoire des Sciences de l'Environnement (LSE) E.N.T.P.E., Rue Audin, 69518 Vaulx-en-Velin Cedex, France

The acid–base and Zn sorption properties of three bacteria, *Cupriavidus metallidurans* CH34, *Pseudomonas putida* ATCC12633, and *Escherichia coli* K12DH5 α , were investigated through an original combination of extended X-ray absorption fine structure (EXAFS) spectroscopy and equilibrium titration studies. Acid–base titration curves of the three strains were fitted with a model accounting for three conceptual reactive sites: an acidic (carboxyl and/or phosphodiester), a neutral (phosphomonoester), and a basic (amine and/or hydroxyl) group. Calculated proton and Zn equilibrium constants and site densities compare with literature data. The nature of Zn binding sites was studied by EXAFS spectroscopy. Phosphoester, carboxyl, and unexpectedly sulfhydryl ligands were identified. Their proportions depended on Zn loading and bacterial strain and were consistent with the titration results. These findings were compared to the structure and site density of the major cell wall components. It appeared that the cumulated theoretical site density of these structures ($<2 \text{ Zn nm}^{-2}$) was much lower than the total site density of the investigated strains ($16\text{--}56 \text{ Zn nm}^{-2}$). These results suggest a dominant role of extracellular polymeric substances in Zn retention processes, although Zn binding to inner cell components cannot be excluded.

Introduction

Many geochemical processes such as sorption, transformation, precipitation, or dissolution of metallic trace elements are microbially mediated (1, 2). Studies dealing with the global transfer characteristics of metals in soils generally consider bacteria as basic biosorbent particles that may either favor the transfer of metals if they are mobile or increase their retention if they form biofilms (3, 4). Such studies address the global reactivity of the bacterial substrate, which reveals that it is generally dependent on pH, redox potential, and dissolved metal concentrations. In this respect, bacterial reactivity to metals is important to assess as it may control the distribution and transport of metals in the environment.

* Corresponding author e-mail: jean.martins@hmg.inpg.fr.

[†] Laboratoire d'Etude des Transferts en Hydrologie et Environnement.

[‡] Environmental Geochemistry Group, LGIT.

[§] Laboratoire des Sciences de l'Environnement (LSE) ENTPE.

Early research by Sherbert (5) or Beveridge and Murray (6) related the bacterial reactivity to the anionic character of specific functional groups situated on membrane components. These authors considered the major cell wall components (e.g., teichoic acids, peptidoglycan, phospholipids) as principally responsible for the overall bacterial reactivity. The determined reactive anionic functional groups were essentially carboxyls (R–COOH), phosphomonoesters (R–OPO₃H₂), phosphodiester ((RO)₂–P(OH)₂), amines (R–NH₃⁺), and hydroxyls (R–OH). On this basis, Fein et al. (7) developed a bacterial sorption model simplifying the variety of these groups to three main site groups differing in acid–base reactivity: acidic sites involving carboxyl and phosphodiester groups ($pK < 4.7$), neutral sites involving phosphomonoester groups (pK values ≈ 7), and basic sites involving hydroxyl and amine groups ($pK > 8$). Using such approaches, the reactivity of various heavy metals (Cu, Cd, Zn, Al, Pb, etc.) with numerous bacterial substrates was assessed (7–14). Yee and Fein (11) found that the metal sorption capacity and reactivity of different Gram-positive and -negative bacteria roughly compare. This finding led them to develop a universal adsorption edge model, which considers similar reactivity for all bacteria. Although helpful in practice, this approach appears surprising on a first look, specifically with regards to the different structures involved in the cell wall of Gram-positive and -negative bacteria. To validate this conceptualization, innovative approaches coupling macroscopic and microscopic studies are needed to assess both reactivity (affinity constants) and structure of reactive sites on bacterial membranes. To date, only a few studies have combined such approaches on such materials (15–17).

The present work aims at determining the reactivity and nature of Zn-binding components of three Gram-negative bacteria of environmental interest (*Cupriavidus metallidurans* CH34, *Pseudomonas putida* ATCC12633, and *Escherichia coli* K12DH5 α). The surface reactivity of these bacteria was assessed macroscopically through proton exchange and zinc adsorption experiments and microscopically through Zn K-edge extended X-ray absorption fine structure (EXAFS) spectroscopy. These results are discussed in light of the composition and structure of bacterial cell walls.

Materials and Methods

Bacterial Cell Preparation and Growth. Three rod-shaped Gram-negative aerobic strains were investigated: the metal tolerant *C. metallidurans* CH34 (formerly *Ralstonia metallidurans* CH34), a *P. putida* strain (ATCC12633) commonly found in natural environments, and *E. coli* K12DH5 α . Three minimum media were used for bacteria cultivation based on their nutritive specificity: a mineral salt medium (MSM) with 1 g L^{-1} acetate for *P. putida*, the M9 medium with 5 g L^{-1} glucose for *E. coli*, and a TRIS salt medium (TSM) with 2 g L^{-1} gluconate for *C. metallidurans*. Compared to rich Luria broth (LB), these mineral media ensure an improved reproducibility of acid–base titrations. The three bacterial strains were grown by shaking at 200 rpm until the late exponential phase (24 h/30 °C) for *E. coli* and *C. metallidurans* and to the stationary phase (50 h/23 °C) for *P. putida*. The cells were then pelleted (9000g), washed, and resuspended 3 times in 10 mM NaCl. Elemental analysis shows that the C/N/P/S elemental contents (% \pm SD of triplicate measurements) for the three strains compare within close limits: C = 45.8 ± 2.1 ; N = 12.0 ± 0.9 ; P = 1.8 ± 0.5 ; and S = 0.54 ± 0.10 . The determination of cell concentrations is detailed in the Supporting Information. The geometric characteristics

of the three strains (Table 1) were obtained from TEM observations (20 keV, 10 000 magnification).

Acid–Base Titration Experiments. Acid–base titrations were performed in a closed vessel under N₂ positive pressure. A total of 50 mL of bacterial suspensions of 2 ± 0.4 g_{DW} L⁻¹ (DW: dry weight) were stirred and maintained at 4 °C (*E. coli* and *C. metallidurans*) or 20 °C (*P. putida*). In the case of *E. coli* and *C. metallidurans*, the potential of the pH electrode did not stabilize within a reasonable time scale at 20 °C, whereas at 4 °C, reproducible measurements were obtained. Titrations were performed from the equilibrium pH of cell suspensions (pH 5–7) toward pH 4 or 10 adding strong acid or base stepwise, respectively. This procedure avoids irreversible effects on bacteria such as cell aggregation and membrane denaturing. The data treatment was based on the proton mass balance

$$[H^+] = \frac{\nu_0[H_I]}{\nu_0 + \nu} + \frac{\nu[H_B]}{\nu_0 + \nu} + \frac{\nu_0[H_S]}{\nu_0 + \nu} + [OH^-]$$

where [H⁺] is the free proton concentration; [H_I] is the analytically known initial concentration of strong acid (positive) or base (negative) added to the reactor; [H_B] is the buret strong acid (positive) or base (negative) concentration; [H_S] is the experimentally assessed concentration of protons released from the weak ligand (i.e., the bacterial substrate); [OH⁻] are the protons generated from water dissociation; ν₀ is the initial reactor volume; and ν is the buret volume added to the reactor. A detailed description is provided in the Supporting Information.

Titration reversibility was studied in duplicate for *P. putida* (data not shown). A good agreement (less than 5% difference) between up and down titrations was observed, indicating a complete reversibility of proton exchange, as demonstrated by several other works (7, 9, 11, 18). A similar behavior was assumed for the other two bacteria. Cell viability performed after each titration experiment revealed always over 70% survival.

Acid–Base Titration Modeling. In modeling, three acid–base exchange sites were discriminated within the investigated pH range following Fein et al. (7), which are noted as:

- (1) acidic site: ≡COOH ↔ ≡COO⁻ + H⁺; 2 ≤ pK_{x-CH} ≤ 6; [T_{x-CH}];
- (2) neutral site: ≡POH ↔ ≡PO⁻ + H⁺; 5.7 ≤ pK_{x-PH} ≤ 7.2; [T_{x-PH}];
- (3) basic site: ≡NH⁺ ↔ ≡N + H⁺; 8 ≤ pK_{x-NH} ≤ 12; [T_{x-NH}].

They are, respectively, representative for carboxyl and phosphodiester (1), phosphomonoesters (2), and hydroxyl and amine (3) functional groups, with x = CM for *C. metallidurans*, x = EC for *E. coli*, and x = PP for *P. putida*. [T_{x-CH}], [T_{x-PH}], and [T_{x-NH}] refer to the total concentrations of these respective sites. Clearly, these three sites are a simplification of the continuous distribution of pK values. The sum of the three terms expresses the total proton exchange capacity of the bacterial strain. A detailed description of the modeling approach is given in the Supporting Information. GRFIT (19), was used to model equilibrium data. This FITEQL substitute enables a visual comparison of fitted and experimental data. In agreement with Fein et al. (14) who showed that acid–base titrations of *Bacillus subtilis* did not allow the discrimination of surface electrostatic effects, our analysis was based on a nonelectrostatic model, which is a simplification of the real processes.

Zn Sorption and EXAFS Spectroscopy. Equilibrium zinc sorption studies were performed at 4 °C in stirred closed vessels (40 mL), I = 10 ± 1 (mM) (i) at fixed total Zn concentration ([T_{Zn}] = 40, 160, or 900 μM) and varying pH (from 3.5 to 8.5) in triplicate and (ii) at fixed pH (3.7 ± 0.1, 5.8 ± 0.1, or 7.8 ± 0.1) and varying [T_{Zn}] (from 1.5 to 760 μM) in duplicate. During the 24 h equilibration time, small aliquots

TABLE 1. Main Characteristics of Bacterial Strains

	enumeration ^b		cell geometry ^c			proton exchange ^{d,e,f}			Zn exchange ^e				
	nb. of cells cells g _{DW} ⁻¹ ± 20%	biomass g _{DW} OD ₆₀₀ ⁻¹ L ⁻¹ ± 20%	protein g cells ⁻¹ ± 20%	length μm ± 10%	diameter μm ± 10%	surface μm ² ± 10%	IEP ^d	pK _{x-CH} ; [T _{x-CH}]	pK _{x-PH} ; [T _{x-PH}]	pK _{x-NH} ; [T _{x-NH}]	log K _{x-CZn}	log K _{x-PZn}	log K _{x-NZn}
<i>C. metallidurans</i>	1.22 × 10 ¹²	0.30		1.2	0.4	1.76	3.5	3.8; 0.42	6.7; 0.12	9.4; 0.45	2.0	4.0	5.2
<i>E. coli</i>	8.55 × 10 ¹¹	0.45		2.1	0.6	4.52	3.3	4.6; 0.25	6.8; 0.071	9.2; 0.25	3.3	5.3	6.5
<i>P. putida</i>	1.21 × 10 ¹²		4.5 × 10 ⁻¹³	3.0	0.6	6.22	3.5	4.4; 0.53	6.5; 0.32	9.7; 0.73	2.2	4.6	5.6

^a [T] in mmol g_{DW}⁻¹. ^b Uncertainties correspond to ± SD (rounded up) calculated from five independent replications. ^c Obtained from TEM (20 keV, × 10 000) observations of fresh cells, considering a cylindrical shape of the cells. ^d IEP = pH of isoelectric point (details on electrophoretic mobility measurements given in the Supporting Information). ^e Conditional constants: at 4 °C (except for *P. putida* proton exchange data: 20 °C) in 10 mM NaCl. ^f Uncertainties are ± 0.2 for pK_{x-PH}, ± 0.8 for pK_{x-CH} and pK_{x-NH}, ± 10% for [T_{x-PH}], and ± 30% for [T_{x-CH}] and [T_{x-NH}].

of acid or base were added when necessary to maintain the initial pH (± 0.1). The vessel opening time was minimized to limit CO₂ intrusion. Control vessels without bacteria were prepared to account for precipitation and/or vial adsorption. Dissolved Zn was quantified by ICP-AES (Perkin-Elmer, Optima 3300 DV). The Phreeqc code (20) was used to model zinc sorption.

EXAFS Zn samples were prepared by equilibrating bacterial suspensions at different total biomass concentrations [T_B] for 24 h with two [T_{Zn}] resulting in different adsorbed Zn concentrations (high and low [Zn_{ads}], Table 2). After equilibrium, the suspension pH was measured, and the cells were centrifuged at 9000g.

Considering the low Zn content of some of the samples (down to 2.3 $\mu\text{mol g}_{\text{DW}}^{-1}$), it was not possible to record them in the hydrated state. For homogeneity, all of them were recorded in the freeze-dried state. Pokrovsky et al. (21) did not observe any difference in Zn speciation between fresh and freeze-dried diatoms. The effect of freeze-drying on Zn speciation was not evaluated, but the redistribution of Zn on different binding sites is unlikely since (i) the removal of water molecules takes place in frozen state and (ii) the cells were not rehydrated thereafter. The bacterial pellets were instantly frozen by plunging the tubes in liquid nitrogen, freeze-dried (Christ, Osterode am Harz, Germany, -52°C , 0.2 mbar), pressed as pellets, and stored in a dry atmosphere before EXAFS measurement. Zn K-edge EXAFS spectra for the bacteria were measured at 100 K on the FAME beamline at the European Synchrotron Radiation Facility (ESRF, Grenoble, France) in fluorescence mode using a 30-element solid-state Ge detector (Canberra) for the diluted samples and in transmission mode using a diode for the most concentrated samples. EXAFS data extraction was done according to standard methods, and EXAFS analysis was performed by linear combinations fits and by standard FEFF simulation for the first shell, as detailed in the Supporting Information.

Results

Surface Proton Exchange. The acid–base titration curves of the three bacteria are presented in Figure 1. The amount of protons exchanged between pH 4 and 10, defined as $\Delta[H_S]$, is 0.99, 0.52, and 1.2 mmol $\text{g}_{\text{DW}}^{-1}$ for *C. metallidurans*, *E. coli*, and *P. putida*, respectively. Thus, the proton sorption capacity of the three strains compares within a factor of 2.3 in this pH range.

The curve for *P. putida* presents three steps in the acidic (4–5.5), neutral (6.4–7.5), and basic (8.5–10) pH ranges, respectively, attesting for the existence of at least three proton exchanging functional groups. For the two other bacteria, no particular change of the slope is observed between pH 5.3 to 8.3, but $\Delta[H_S]$ is still significant within these pH limits. Indeed, $\Delta[H_S]$ between pH 5.3 to 8.3 equals 0.15 mmol/ g_{DW} for both bacteria, which represents 15 and 29% of $\Delta[H_S]$ exchanged between pH 4 and 10 for *C. metallidurans* and *E. coli*, respectively. This indicates that a neutral proton exchanger also exists for these bacteria. Outside the 4–10 pH range, the slopes of the three curves are not null, indicating that proton exchange reactions occur outside the experimentally available pH range and involving an underestimation of the effective total site concentration of acidic and basic groups. Thus, the total proton exchange capacity is higher than that calculated from the pH 4–10 $\Delta[H_S]$ reading. $\text{p}K_{\text{PP-PH}}$ situates at the inflection point around pH 7. The $\Delta[H_S]$ reading between pH 6 and 8 is thus an approximation of the phosphomonoester total site concentration ($[T_{\text{X-PH}}]$ mmol $\text{g}_{\text{DW}}^{-1}$) of the three bacteria: $[T_{\text{PP-PH}}] \cong 0.32$, $[T_{\text{CM-PH}}] \cong 0.12$, and $[T_{\text{EC-PH}}] \cong 0.07$. Solid lines in Figure 1 are the best fits obtained, and the corresponding $\text{p}K$ and $[T]$ parameters are given in Table 1. $[T_{\text{X-PH}}]$ was first optimized and then

TABLE 2. EXAFS Results for Bacterial Samples and Zn Reference Compounds

strain or sample ^c	sample characteristics			first shell structural parameters ^a			proportion (%) for each type of ligand determined by LCFs ^b						
	pH (± 0.1)	$[T_B]$ g L ⁻¹	$[Zn_{ads}]$ $\mu\text{mol g}_{\text{DW}}^{-1}$	atom	CN	R (\AA)	σ^2 (\AA^2)	NSS	Zn-sorbed hydroxylapatite	Zn-humic acid	Zn-cysteine (L/M = 5)	sum	NSS
<i>C. metallidurans</i>	6.5	2.5	2.9	{ O	2.8	1.97	0.010	1.0	61 \pm 6	0	49 \pm 5	110	5.7
<i>C. metallidurans</i>	4.8	1.2	10.8	{ S	2.5	2.31	0.010	1.4	54 \pm 10	57 \pm 7	0	111	3.6
<i>E. coli</i>	6.4	4.0	2.3	{ O	3.1	1.97	0.009	1.0	81 \pm 7	19 \pm 14	8 \pm 6	108	4.6
<i>E. coli</i>	5.6	7.7	108	{ S	1.5	2.28	0.010	1.3	88 \pm 9	24 \pm 9	0	112	4.1
<i>P. putida</i>	6.5	1.7	5.9	{ O	5.1	1.97	0.008	2.0	72 \pm 4	32 \pm 4	0	104	3.7
<i>P. putida</i>	5.6	2.5	362	{ O	6.0	2.02	0.005	1.4	59 \pm 20	44 \pm 19	0	103	3.1
Zn cysteine (L/M = 5)			≈ 3200	{ S	1.4	1.99	0.010	0.7					
Zn cysteine (L/M = 10)				{ S	3.3	2.32	0.010						
				S	4.5	2.35	0.007	1.2					

^a CN: coordination number; R: interatomic distance (\AA); σ^2 : Debye–Waller disorder factor (\AA^2); residual: $\text{NSS} = \sum [k^2 \chi(k) / k_{\text{exp}} - k^2 \chi(k) / k_{\text{ref}}]^2 / \sum [k^2 \chi(k) / k_{\text{ref}}]^2 \times 100$. For the first shell simulations, an amplitude reduction factor (S_0^2) of 0.9 was used for all fits. Estimated errors on R and CN are 0.02 \AA and 20%, respectively. ^b The proportions of the ligands are given as mean \pm SD obtained from the best simulations. ^c The bacterial samples were recorded in a freeze-dried state. L/M corresponds to the ligand/metal molar ratio used to prepare the reference compounds (see Supporting Information).

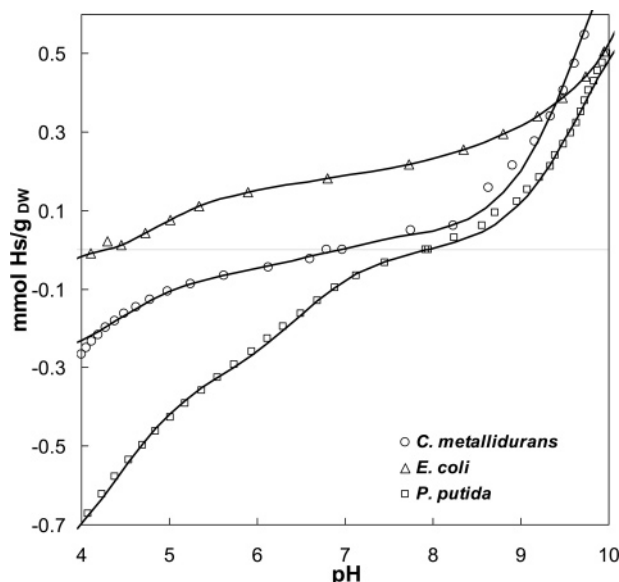


FIGURE 1. Acid–base titration curves for *C. metallidurans*, *E. coli*, and *P. putida*. Symbols and solid lines refer to measured and calculated data, respectively (Table 1).

held constant during adjustments of the five remaining variables. The uncertainties on pK_{x-PH} and $[T_{x-PH}]$ are relatively low (± 0.2 log units and $\pm 10\%$, respectively), and the fitted pK_{x-PH} values for the three bacteria are close (Table 1). Obviously, pK and $[T]$ uncertainties for acidic (x_{-CH}) and basic sites (x_{-NH}) are higher (± 0.8 log units and $\pm 30\%$, respectively) since data are not available at extreme pH values. Both pK and $[T]$ values compare to previously published data for *Enterobacteriaceae* (12), with $[T] = 0.50 \pm 0.07$ for the acidic site ($pK 4.3 \pm 0.2$), 0.22 ± 0.06 $\text{mmol g}_{\text{DW}}^{-1}$ for the neutral site ($pK 6.9 \pm 0.5$), and 0.55 ± 0.02 $\text{mmol g}_{\text{DW}}^{-1}$ for the basic site ($pK 8.9 \pm 0.5$). Close values were also observed for *Picocyanobacteria* (13): $0.26\text{--}0.74$ ($pK 4.8\text{--}5.0$); $0.19\text{--}0.44$ ($pK 6.6\text{--}6.7$); and $0.25\text{--}0.48$ $\text{mmol g}_{\text{DW}}^{-1}$ ($pK 8.8\text{--}8.7$). Yee and Fein (11) found higher $[T]$ values for Gram-negative and -positive bacteria: $0.9\text{--}3.1$ ($pK 5.0 \pm 0.2$), $0.4\text{--}1.4$ ($pK 7.2$), and $0.6\text{--}2.9$ $\text{mmol g}_{\text{DW}}^{-1}$ ($pK 9.7$). Contrarily, Haas et al. (9) measured lower $[T]$ values for *Shewanella putrefaciens*: 0.03 ($pK 5.16 \pm 0.04$), 0.01 ($pK 7.22 \pm 0.15$), and 0.04 $\text{mmol g}_{\text{DW}}^{-1}$ ($pK 10.04 \pm 0.67$).

Zinc Sorption. Zinc sorption isotherms are presented in Figure 2. As expected, $[Zn_{\text{ads}}]$ increases with pH and Zn in solution ($[Zn_{\text{aq}}]$). For all three bacteria (Figure 2A) and at three different pH values (Figure 2B), the $[Zn_{\text{ads}}]$ versus $[Zn_{\text{aq}}]$ curve slope decreases progressively with an increasing $[Zn_{\text{aq}}]$, suggesting a gradual saturation of surface reactive sites. Figure 2A shows that at constant pH (5.8 ± 0.1), the cell reactivity to Zn follows the order $P. putida \approx E. coli > C. metallidurans$, within a 1 log unit difference in reactivity. At high Zn loading, this difference tends to decrease, suggesting similar Zn-total site concentrations. Zinc sorption isotherms at varying pH values are given in Figure 3. At pH 5.8 ± 0.1 and comparable total zinc $[T_{\text{Zn}}]$ and biomass $[T_{\text{B}}]$ concentrations, *E. coli* sorbs about 3–4 times more zinc than *C. metallidurans*, as already observed in Figure 2A.

The PhreeqC code was used to model zinc sorption, assuming that the sorption is reversible (7, 9, 11, 18) and that metals compete with protons on acid–base reactive sites. A 1:1 stoichiometric ratio is considered for complex interactions of cations with bacterial sites: (acidic site: $\equiv\text{COO}^- + \text{Zn}^{2+} \leftrightarrow \equiv\text{COOZn}^+$; $\log K_{x-CZn}$; neutral site: $\equiv\text{PO}^- + \text{Zn}^{2+} \leftrightarrow \equiv\text{POZn}^+$; $\log K_{x-PZn}$; and basic site: $\equiv\text{N} + \text{Zn}^{2+} \leftrightarrow \equiv\text{NZn}^{2+}$; $\log K_{x-NZn}$).

Commonly, it is considered that basic hydroxyl and amine sites do not significantly contribute to cation adsorption.

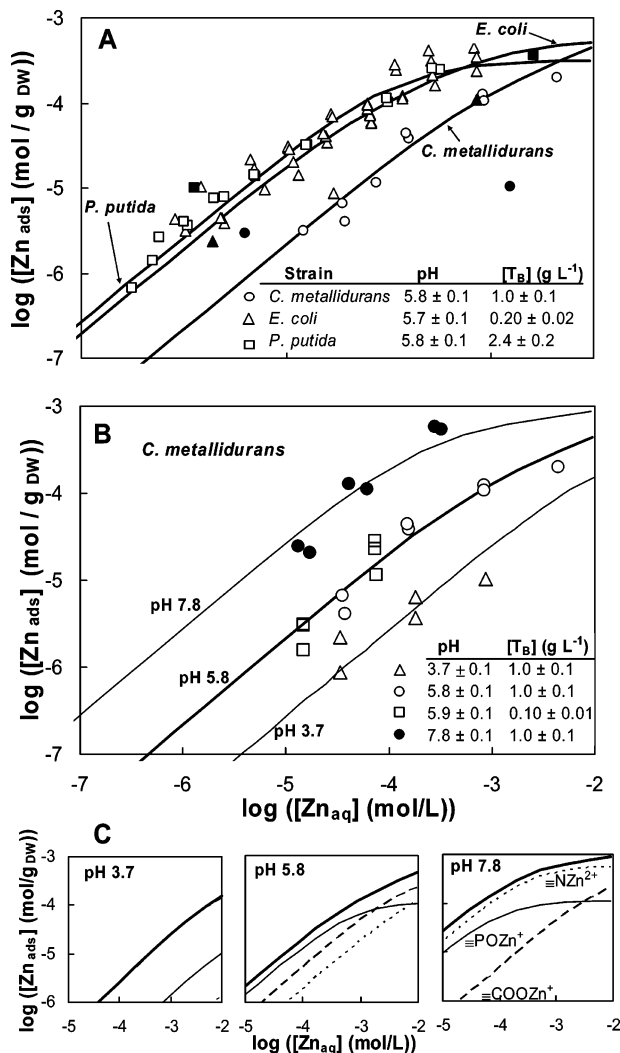


FIGURE 2. (A) Calculated (solid lines, model parameters are given in Table 1) and measured Zn sorption isotherms at pH 5.8 for *C. metallidurans*, *E. coli*, and *P. putida*. Black symbols refer to low and high Zn concentration EXAFS samples: pH, biomass $[T_{\text{B}}]$ (g L^{-1}), and total Zn concentration $[T_{\text{Zn}}]$ (mM) for these samples are 4.8 ± 0.1 , 1.2 ± 0.1 , and 1.2 ± 0.2 , and 6.5 ± 0.1 , 2.5 ± 0.2 , and 0.010 ± 0.001 for *C. metallidurans*; 5.6 ± 0.1 , 7.7 ± 0.8 , and 1.2 ± 0.2 , and 6.4 ± 0.1 , 4.0 ± 0.4 , and 0.010 ± 0.001 for *E. coli*; and 5.6 ± 0.1 , 2.5 ± 0.2 , and 4.1 ± 0.4 ; and 6.5 ± 0.1 , 1.7 ± 0.2 , and 0.010 ± 0.001 for *P. putida*. (B) Measured and calculated Zn sorption isotherm for *C. metallidurans* at pH 3.7, 5.8 (similar to panel A), and 7.8. (C) Calculated Zn distributions for phosphoester ($\equiv\text{POZn}^+$, thin black lines), carboxyl ($\equiv\text{COOZn}^+$, dashed lines), and amine ($\equiv\text{NZn}^{2+}$, dotted lines) sorption sites plotted at pH 3.7 (left), 5.8 (center), and 7.8 (right) using *C. metallidurans* constants. The sum of the three contributions (thick black line) represents the total sorbed Zn curve such as presented in panels A and B. Note that the chosen axes and units ($\text{mol g}_{\text{DW}}^{-1}$ vs mol L^{-1}) are permitted to fit the data independently from biomass concentration.

The present dataset covers relatively large pH (3.5–8.5) and $[Zn_{\text{aq}}]$ ($10^{-5.8}$ to $10^{-3.0}$ mol L^{-1}) ranges. Considering only Zn sorption on $\equiv\text{POH}$ and $\equiv\text{COOH}$ sites, it was not possible to fit the gap between isotherms at pH 5.8 and 7.8 (Figure 2B). These sites are deprotonated at high pH values, meaning that metal adsorption is pH independent. Thus, if complexation on basic sites is not considered, the fitted curves at pH 5.8 and 7.8 almost overlap. The introduction of basic Zn-complexation sites led to an adequate data fit for *C. metallidurans* (Figure 2B). On this basis, we also considered Zn complexation on the three functional groups for the *E. coli* and *P. putida* datasets. The $\log K_{\text{PP-NZn}}$ and $\log K_{\text{PP-PZn}}$

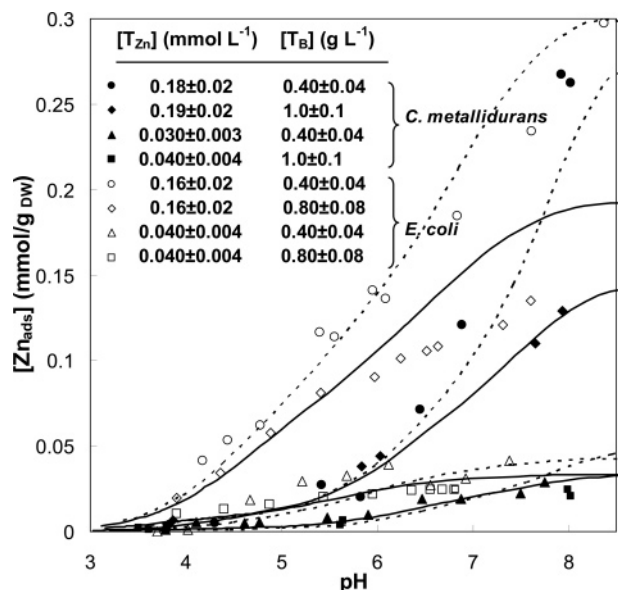


FIGURE 3. *E. coli* and *C. metallidurans* Zn-sorption experiments performed at varying pH. Calculated solid lines refer to full symbol data, and calculated dashed lines refer to empty symbol data. Note that for clarity, only data obtained at $[T_{Zn}]$ 0.04 and 0.18 mmol L⁻¹, for *C. metallidurans*, are presented. Data at 0.9 mmol L⁻¹ were not presented but were similarly well-fitted. Note that modeling depends on biomass concentrations in this representation ($[Zn_{ads}]$ vs pH).

constants were set as close as possible to those of *C. metallidurans* and *E. coli*. The determined $\log K_{x-pZn}$ and $\log K_{x-CZn}$ values compare to published data on *Enterobacteriaceae* (12), *B. subtilis* (22), and *Rhodococcus erythropolis* (8).

The distribution of Zn sorption sites can be assessed from the model curves given in Figure 2C. This speciation scheme relates to the largest *C. metallidurans* dataset and is considered also conceptually valid for the two other bacteria. At low pH, the acidic $\equiv\text{COOH}$ site is the dominant Zn complexing group (Figure 2C, left). At intermediate pH (5.8), the dominant complexing group depends on surface coverage (Figure 2C, center): at low surface coverage, most Zn is bound to the $\equiv\text{POH}$ site (phosphomonoester groups), but this site of relatively low capacity is rapidly saturated, and the excess Zn is then complexed to acidic carboxyl groups. At pH 7.8, the basic $\equiv\text{NH}^+$ site is the only and dominant Zn sorbent (Figure 2C, right).

EXAFS Analysis. Zn K-edge EXAFS spectroscopy was applied to independently characterize the Zn-binding sites at low and high Zn concentrations for the three bacteria (position of the EXAFS samples on the Zn adsorption isotherms in Figure 2A). The spectra for the most concentrated samples (*P. putida*, 362 $\mu\text{mol g}_{\text{DW}}^{-1}$ Zn; *E. coli*, 108 $\mu\text{mol g}_{\text{DW}}^{-1}$ Zn; and *C. metallidurans*, 10.8 $\mu\text{mol g}_{\text{DW}}^{-1}$ Zn) contain a dominant single frequency typical of Zn bound to oxygen-containing ligands as found in Zn malate and/or Zn-sorbed hydroxylapatite (Figure 4). The spectra for the most diluted Zn samples (*C. metallidurans*, 2.9 $\mu\text{mol g}_{\text{DW}}^{-1}$ Zn and *E. coli*, 2.3 $\mu\text{mol g}_{\text{DW}}^{-1}$ Zn) are not in phase with the previous ones. Particularly, their second and third oscillation maxima are slightly shifted to lower wavenumbers (left and middle vertical lines in Figure 4). These shifts are in line with the corresponding oscillation maxima for Zn cysteine (prepared with a ligand/metal ratio (L/M) = 5). However, the fourth oscillation maximum for this Zn cysteine reference is not visible on the bacterial spectra (right vertical line in Figure 4). It is possible that the combination of Zn-S and Zn-O contributions cancel each other around 9.1 Å in these two low Zn loaded samples. The spectrum for *P. putida*, 5.9 $\mu\text{mol g}_{\text{DW}}^{-1}$ Zn, is intermediate between the most concentrated

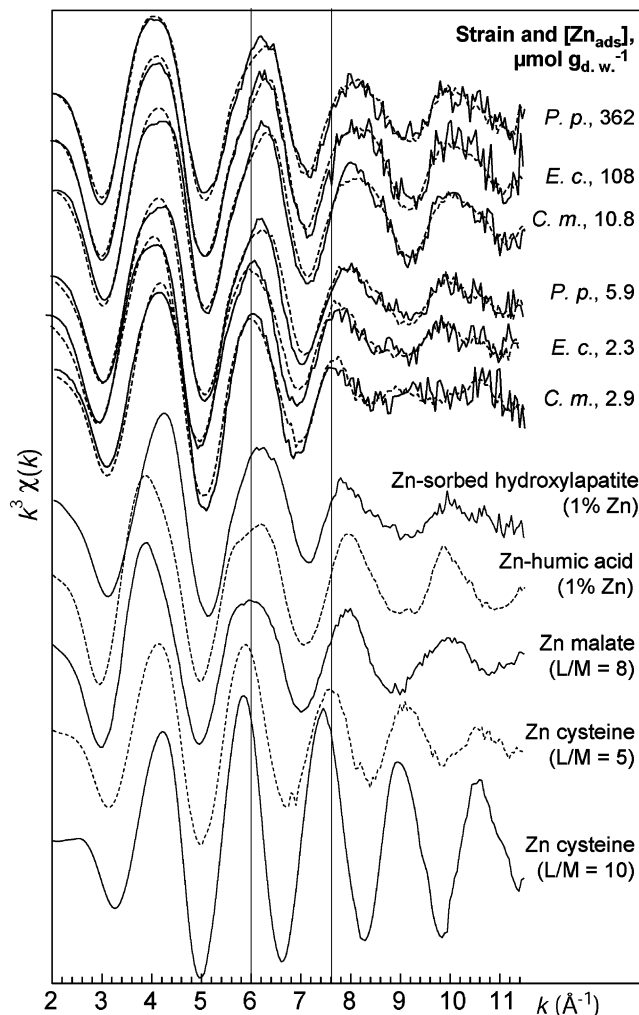


FIGURE 4. EXAFS spectra for the freeze-dried Zn-sorbed bacteria and Zn reference compounds (see Supporting Information). Dotted lines represent linear combination fits. The proportions of Zn species are given in Table 2.

and the most diluted samples. These spectra were decomposed by linear combination fits (LCFs, Figure 4 and Table 2) using a library of Zn reference spectra including simple (e.g., Zn complexed to simple organic acids) and complex compounds (e.g., Zn complexed with humic acids). The references and their significance are given in the Supporting Information. Simulations using simple compounds yielded unsatisfactory results, and best fits were obtained with two- to three-component combinations of Zn-sorbed hydroxylapatite, Zn-humic acid complex, and Zn-cysteine (L/M = 5) references. In the first reference, Zn is bound to phosphate surface sites (23). This spectrum is poorly structured, suggesting multiple and/or disordered Zn local environments. The Zn phosphomonoester reference Zn phytate provided weaker fits, and Zn-phosphodiester structures were not tested. However, EXAFS spectroscopy is probably not sensitive enough to distinguish between phosphate, phosphomonoester, and phosphodiester ligands in complex systems since the nature of the Zn nearest and next-nearest neighbors would be identical (O and P, respectively). Thus, this mineral reference is considered as a proxy for a distribution of phosphoester groups of different geometries. Humic acids contain a distribution of carboxyl, phenol, and hydroxyl sites. At the pH used for standards and bacterial sample preparation (below 6.5), the phenol and hydroxyl sites are not deprotonated. Therefore, the second reference can be equated to a distribution of Zn-carboxyl sites. In the third reference (Zn-

cysteine, $L/M = 5$), the metal is bound to sulfhydryl and carboxyl and/or amine ligands. No good simulations were obtained with ZnS or with the other Zn-cysteine reference ($L/M = 10$) in which Zn is bound to S atoms only. This suggests the presence of mixed environments in the bacterial cell walls, with Zn bound to sulfhydryl and carboxyl and/or amine ligands. LCFs results (Table 2) show that Zn phosphoester complexes predominate in all samples except *C. metallidurans*, $10.8 \mu\text{mol Zn g}_{\text{DW}}^{-1}$, and *P. putida*, $362 \mu\text{mol Zn g}_{\text{DW}}^{-1}$, which contain equivalent amounts of Zn-carboxyl and Zn-phosphoester complexes. LCFs indicate that Zn-cysteine type environments are present in *C. metallidurans* and *E. coli* at low Zn loading, but they are not detected at higher Zn loading. They are probably still present but representing less than 5–10% of total Zn due to the predominance of Zn-carboxyl and Zn-phosphoester complexes. Sulfhydryl ligands are not detected in *P. putida* samples. Considering that the S total contents are comparable for the three bacteria (see Materials and Methods), this suggests that the accessibility of Zn to the sulfur groups decreases in the order *C. metallidurans* \gg *E. coli* \gg *P. putida* (~ 0) in our experimental conditions.

The structure of the first coordination shell was studied in more detail by FEFF simulations (Table 2 and Figure S3 in Supporting Information). The results show the presence of 2.5 and 1.5 S atoms in the coordination sphere of Zn for *C. metallidurans* and *E. coli* at low Zn loading, respectively, the rest being O atoms. A simple calculation (see Supporting Information) shows that sulfur atoms bound to Zn represent 4.3 and 2.1% of the total S content, respectively. Compared to the estimated total ion exchange capacity of the bacteria (0.99 and $0.571 \text{ mmol g}_{\text{DW}}^{-1}$, Table 1), sulfhydryl sites represent only 0.73 and 0.60%, respectively. Therefore, these sites cannot be taken into account in the titration experiments.

In the other samples, oxygen is the only Zn neighbor. Zn–O distances range between 1.97 and 2.02 Å, which suggests a mixture of tetrahedral and octahedral environments (24). These distances should be considered with care since the freeze-drying treatment might modify the geometry of the Zn local environment, although the nature of the Zn binding groups should not be affected (see Materials and Methods). The simulation of the second shell did not yield satisfactory fits, probably because of the presence of mixed-types of Zn ligands. Therefore, to determine the most probable configuration of Zn in our samples, a screening of known structures containing Zn-phosphoester and Zn-carboxyl moieties (Cambridge Structural Database) was realized. For P ligands, Zn is bound to only one oxygen atom of the phosphate group (monodentate) in 99% of the structures and to two oxygen atoms of the same phosphate group (bidentate) in the last percent. Similarly, for carboxyl ligands, Zn is bound to one oxygen atom of the COOH group (monodentate) in 90% of the structures and bidentate in the last 10%. Therefore, the corner sharing configuration for Zn–P sites and monodentate Zn–COOH bonds are the most likely.

The identification of phosphoester and carboxyl groups as Zn binding sites are in agreement with previous works on similar systems (17). To our knowledge, Zn-sulfhydryl interactions are evidenced for the first time in bacterial samples. Also, the order of Zn affinity: sulfhydryl > phosphoester > carboxyl obtained from EXAFS compares with the titration results: phosphoester > carboxyl (sulfhydryl sites are not detectable in titration experiments). This is in agreement with a previous study showing a higher affinity of Zn for phosphate than for carboxyl groups in *Penicillium chrysogenum* (24).

Discussion

At pH 5.8, the maximum measured Zn loadings for the three bacteria are about $0.2 \text{ mmol g}_{\text{DW}}^{-1}$ (Figures 2 and 3). Using

the cell geometric data from Table 1, the corresponding calculated site densities are 31, 56, and 16 Zn nm^{-2} , for *E. coli*, *C. metallidurans*, and *P. putida*, respectively. Reactive site densities measured on minerals are much smaller: in the $1 - 4 \text{ Zn nm}^{-2}$ range. Geometrically, it is not possible, for steric reasons, to adsorb on a surface more than 4 Zn nm^{-2} without forming polynuclear complexes (25). Thus, Zn ions sorbed on biomass are undoubtedly localized in different layers or even in different compartments. To validate this Zn distribution over the modeled sites, we investigated the theoretical reactivity of the major cell wall components, based on the assumption that each acid–base reactive group in these structures fixes one Zn atom. The well-characterized membrane structure of *E. coli* was used as a model for the membranes of the studied bacteria (Figure 5).

First, lipopolysaccharides (LPS) are chain molecules evolving from the outer membrane composed of two parts in *E. coli*, a common lipid A base to which links a strain-specific polysaccharide containing reactive phosphomonoester and carboxyl groups (26). The lipid A contains hydrophilic chains attached to two esterified glucosamines, each linked to a reactive phosphomonoester $\equiv\text{OPO}_3\text{H}_2$ functional group (Figure 5). The polysaccharide chains of *E. coli* DH5 α (this study) contains 10 sugars with five phosphomonoester and two carboxyl groups. Thus, seven Zn atoms may be fixed along a LPS unit, which covers approximately 50 nm^2 of the membrane surface (R. Geremia, personal communication). The calculated site density thus equals 0.14 Zn nm^{-2} . Obviously, LPS cannot account for the measured Zn load. Moreover, the carboxyl groups contained in O-Antigens (present in other Gram-negative bacteria) are not zinc and proton reactive (27).

Second, phospholipids are composed of two hydrophobic hydrocarbon chains bound to a glycerol unit to which a hydrophilic headgroup attaches. The *E. coli* headgroup is composed of phosphatidyl ethanolamine containing two acid–base reactive sites (amine and phosphodiester group; Figure 5); thus, two Zn atoms may be fixed. In one phospholipid unit accounting for approximately 5 nm^2 , the maximal site density is 0.4 Zn nm^{-2} , much higher than the LPS site density (0.14 Zn nm^{-2}). Therefore, the hypothesis favoring a maximal site density would be a membrane composed of four superimposed phospholipid layers. On this basis (i.e., considering that one functional group fixes one Zn atom), the calculated total Zn sorption capacity is 1.6 Zn nm^{-2} . Binder and Zschörnig (28) have shown by IR spectroscopy on synthetic lipids that Zn cations may bridge two or more phospholipids. Such stoichiometric relations would lead to an even lower Zn sorption capacity. In summary, the sorption capacity of LPS and phospholipids clearly cannot account for the measured high Zn load ($16 - 56 \text{ Zn nm}^{-2}$). Thus, further components must be considered.

Third, the peptidoglycan (PG) network situated in the periplasmic space is a rigid structure composed of two sugar molecules linked to a tetrapeptide (Figure 5). It contains three carboxyl and one amine group. The terminal D-alanine carboxyl group ($\text{p}K_{\text{a}} 2.4$) forms the interpeptide bond to the amine group of the meso-diaminopimelic acid and is consequently considered not Zn-reactive. The two other carboxyl groups, belonging to D-glutamic acid ($\text{p}K_{\text{a}} 4.1$) and the meso-diaminopimelic acid, may potentially fix two Zn atoms. Considering an area of 10 nm^2 for one PG unit, 0.2 Zn nm^{-2} may be linked to one sheet of PG leading to a theoretical maximum membrane reactivity of 1.8 Zn nm^{-2} , still far from the measured Zn load.

Fourth, the most external cell wall component is the exopolysaccharide (EPS) layer that forms a capsule around the bacteria. It consists of long sugar chains, sometimes containing (i) K-Antigens whose synthesis is enhanced under stress such as starvation or toxic environmental conditions

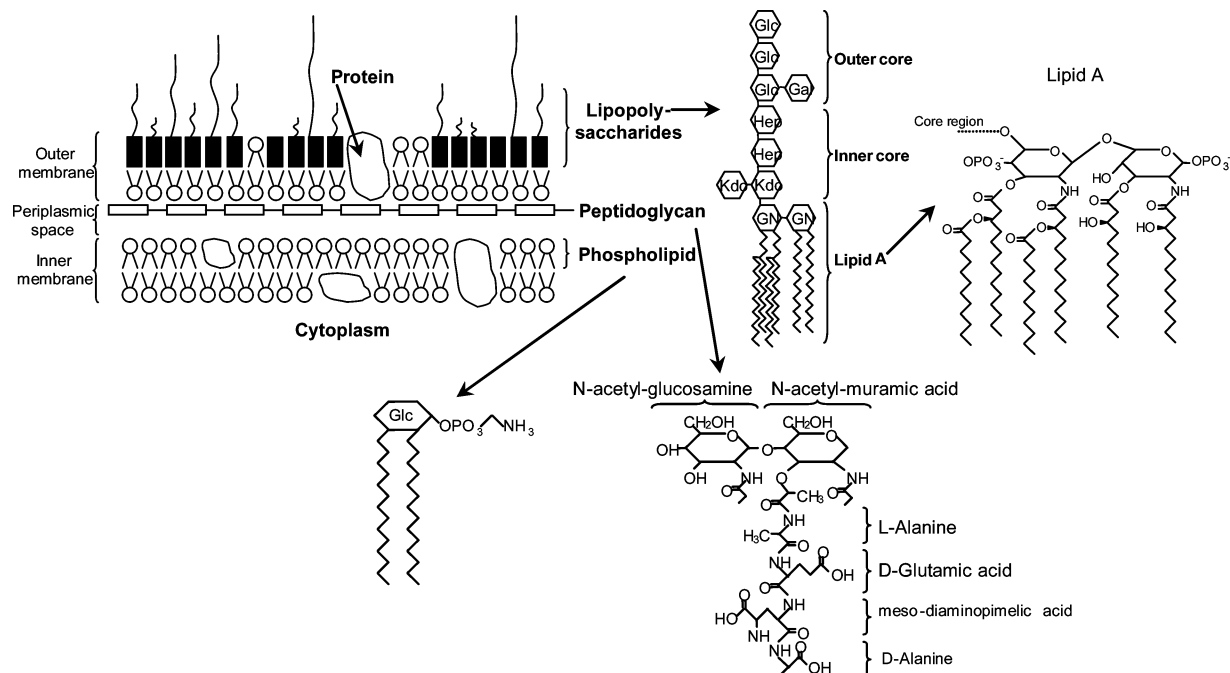


FIGURE 5. Schematic representation of the major reactive components of *E. coli* cell wall (adapted from Kramer et al. (26) and Kadrmas et al. (27)).

(29) and colanic acid. These two components contain reactive carboxyl groups whose amount is difficult to evaluate. These EPS may retain various molecules exuded by the bacteria including nucleic acids, proteins, polysaccharides, and lipids (30). This entity forms the so-called extracellular polymeric substances (EPS^{bis}) and may strongly increase the sorption capacity of bacteria. Matsukawa et al. (31) showed that the EPS^{bis} of *Pseudomonas aeruginosa* biofilms contained up to 80% of nucleic acids. Although EPS^{bis} of planktonic bacteria are known to be less developed, the presence of nucleic acids may contribute to the pool of phosphoester groups evidenced by EXAFS and titrations, and whose amount cannot be explained by the other cell wall components. Sulfhydryl groups identified by EXAFS may belong to proteins of the inner or outer membranes and/or to S-containing compounds possibly present in the EPS^{bis}.

In conclusion, extracellular polymeric substances of the Gram-negative bacteria studied here play a dominant role in Zn retention processes as compared to the other membrane cell components. Besides Zn binding to the EPS^{bis}, the entry of Zn inside the cells and binding to intracellular components cannot be excluded. However, this phenomenon is probably limited since metal sorption on bacteria in similar conditions has been often shown to be reversible (7, 9, 11, 18). Further spectroscopic and thermodynamic characterization of isolated extracellular and intracellular compartments should help to better evaluate their respective role in metal retention by microorganisms.

Acknowledgments

This research was supported by the Programme National Sols et Erosion, ACI Ecologie Quantitative, and ADEME. The authors acknowledge the ESRF for the provision of beamtime, N. Geoffroy and O. Proux for assistance during EXAFS measurements, and S. Beauchemin and F. Panfili for Zn reference spectra. They also thank B. Causse, R. Geremia, and J.B. Fein for fruitful discussions and M. Mergeay and J. Coves.

Supporting Information Available

Experimental and modeling procedures of the titration study, as well as the EXAFS data analysis, with a description of the

database used to fit the data. This material is available free of charge via the Internet at <http://pubs.acs.org>.

Literature Cited

- Ehrlich, H. L. Microbes and metals. *Appl. Microbiol. Biotechnol.* **1997**, *48*, 687–692.
- Ledin, M. Accumulation of metals by microorganisms—processes and importance for soil systems. *Earth Sci. Rev.* **2000**, *51*, 1–31.
- Guiné, V.; Martins, J.; Gaudet, J. P. Facilitated transport of heavy metals by bacterial colloids in sand columns. *J. Phys. IV* **2003**, *107*, 593–596.
- Muris, M.; Delolme, C.; Gaudet, J. P.; Spadini, L. Assessment of biofilm destabilization and consequent facilitated zinc transport. *Water Sci. Technol.* **2005**, *51*, 21–28.
- Sherbert, G. V. *The Biophysical Characterization of the Cell Surface*; Academic Press: London, 1978.
- Beveridge, T. J.; Murray, R. Sites of metal deposition in the cell wall of *Bacillus subtilis*. *J. Bacteriol.* **1980**, *141*, 876–887.
- Fein, J. B.; Daughney, C.; Yee, N.; Davis, T. A. A chemical equilibrium model for metal adsorption onto bacterial surfaces. *Geochim. Cosmochim. Acta* **1997**, *61*, 3319–3328.
- Plette, A. C. C.; Benedetti, M. F.; Van Riemsdijk, W. H. Competitive binding of protons, calcium, cadmium, and zinc to isolated cell walls of a Gram-positive soil bacterium. *Environ. Sci. Technol.* **1996**, *30*, 1902–1910.
- Haas, J. R.; Dichristina, T. J.; Wade, R. J. Thermodynamics of U(VI) sorption onto *Shewanella putrefaciens*. *Chem. Geol.* **2001**, *180*, 33–54.
- Sokolov, I.; Smith, D.; Henderson, G.; Gorby, Y.; Ferris, F. Cell surface electrochemical heterogeneity of the Fe(III)-reducing bacteria *Shewanella putrefaciens*. *Environ. Sci. Technol.* **2001**, *35*, 341–347.
- Yee, N.; Fein, J. B. Cd adsorption onto bacterial surfaces: a universal adsorption edge? *Geochim. Cosmochim. Acta* **2001**, *65*, 2037–2042.
- Ngwenya, B. T.; Sutherland, I. W.; Kennedy, L. Comparison of the acid–base behaviour and metal adsorption characteristics of a gram-negative bacterium with other strains. *Appl. Geochem.* **2003**, *18*, 527–538.
- Dittrich, M.; Sibling, S. Cell surface groups of two picocyanobacteria strains studied by zeta potential investigations, potentiometric titration, and infrared spectroscopy. *J. Colloid Interface Sci.* **2005**, *286*, 487–495.
- Fein, J. B.; Boily, J.-F.; Yee, N.; Gorman-Lewis, D.; Turner, B. F. Potentiometric titrations of *Bacillus subtilis* cells to low pH and comparison of modeling approaches. *Geochim. Cosmochim. Acta* **2005**, *69*, 1123–1132.

- (15) Kelly, S. D.; Kemner, K. M.; Fein, J. B.; Fowle, D. A.; Boyanov, M. I.; Bunker, B. A.; Yee, N. X-ray absorption fine structure determination of pH-dependent U-bacterial cell wall interactions. *Geochim. Cosmochim. Acta* **2002**, *66*, 3855–3871.
- (16) Boyanov, M. I.; Kelly, S. D.; Kemner, K. M.; Bunker, B. A.; Fein, J. B.; Fowle, D. A. Adsorption of cadmium to *Bacillus subtilis* bacterial cell walls: A pH-dependent X-ray absorption fine structure spectroscopy study. *Geochim. Cosmochim. Acta* **2003**, *67*, 3299–3311.
- (17) Toner, B.; Manceau, A.; Marcus, M. A.; Millet, D. B.; Sposito, G. Zinc sorption by a bacterial biofilm. *Environ. Sci. Technol.* **2005**, *39*, 8288–8294.
- (18) Fowle, D. A.; Fein, J. B. Competitive adsorption of metal cations onto two Gram-positive bacteria: Testing the chemical equilibrium model. *Geochim. Cosmochim. Acta* **1999**, *63*, 3059–3067.
- (19) Ludwig, C. GRFIT: A program for solving speciation problems, evaluation of equilibrium constants, concentrations, and their physical parameters, Ph. D. Thesis, University of Berne, 1992.
- (20) Parkhurst, D. L.; Appelo, C. A. J. User's guide to Phreeqc (version 2), A computer program for speciation batch-reaction, one-dimensional transport, and inverse geochemical calculations. *Water Resour. Invest. Rep.* **1999**, *99*, 4259.
- (21) Pokrovsky, O. S.; Pokrovski, G. S.; Gelabert, A.; Schott, J.; Boudou, A. Speciation of Zn associated with diatoms using X-ray absorption spectroscopy. *Environ. Sci. Technol.* **2005**, *39*, 4490.
- (22) Fein, J. B.; Martin, A. M.; Wightman, P. G. Metal adsorption onto bacterial surfaces: Development of a predictive approach. *Geochim. Cosmochim. Acta* **2001**, *65*, 4267–4273.
- (23) Panfili, F.; Manceau, A.; Sarret, G.; Spadini, L.; Kirpichtchikova, T.; Bert, V.; Laboudigue, A.; Marcus, M.; Ahamdach, N.; Libert, M. The effect of phytostabilization on Zn speciation in a dredged contaminated sediment using scanning electron microscopy, X-ray fluorescence, EXAFS spectroscopy, and principal components analysis. *Geochim. Cosmochim. Acta* **2005**, *69*, 2265–2284.
- (24) Sarret, G.; Manceau, A.; Spadini, L.; Roux, J. C.; Hazemann, J. L.; Soldo, Y.; Eybert-Bérard, L.; Menthonnex, J. J. EXAFS determination of Pb, Zn complexing sites of *Penicillium chrysogenum* cell walls. *Environ. Sci. Technol.* **1998**, *32*, 1648–1655.
- (25) Spadini, L.; Schindler, P. W.; Charlet, L.; Manceau, A.; Ragnarsdóttir, K. V. Hydrous ferric oxide: evaluation of Cd–HFO surface complexation models combining Cd–K EXAFS data, potentiometric titration results, and surface site structures identified from mineralogical knowledge. *J. Colloid Interface Sci.* **2003**, *266*, 1–18.
- (26) Kramer, R. A.; Brandenburg, K.; Vandeputte-Rutten, L.; Werkhoven, M.; Gros, P.; Dekker, N.; Egmond, M. Lipopolysaccharide regions involved in the activation of *Escherichia coli* outer membrane protease OmpT. *Eur. J. Biochem.* **2002**, *269*, 1746–1752.
- (27) Kadmas, J. L.; Raetz, C. R. H. Enzymatic synthesis of lipopolysaccharide in *Escherichia coli*. *J. Biol. Chem.* **1998**, *273*, 2799–2807.
- (28) Binder, H.; Zschörnig, O. The effect of metal cations on the phase behavior and hydration characteristics of phospholipid membranes. *Chem. Phys. Lipids* **2002**, 39–61.
- (29) Whitfield, C.; Roberts, I. Structure, assembly, and regulation of expression of capsules in *Escherichia coli*. *Mol. Microbiol.* **1999**, *31*, 1307–1319.
- (30) Wingender, J.; Neu, T.; Flemming, H., Eds. *Microbial Extracellular Polymeric Substances—Characterization, Structure, and Function*; Springer-Verlag: Berlin, 1999.
- (31) Matsukawa, M.; Greenberg, E. P. Putative exopolysaccharide synthesis genes influence *Pseudomonas aeruginosa* biofilm development. *J. Bacteriol.* **2004**, *186*, 4449–4456.

Received for review May 24, 2005. Revised manuscript received December 21, 2005. Accepted December 21, 2005.

ES050981L